GPS Solutions (2022) 26:102
https://doi.org/10.1007/s10291-022-01286-4

ORIGINAL ARTICLE

Real-time carrier observation quality control algorithm for precision orbit determination of LEO satellites

Gongwei Xiao[1] · Genyou Liu[2] · Jikun Ou[2] · Chongchong Zhou[2] · Zaimin He[1] · Runjing Chen[3] · Aizhi Guo[2] · Zhouming Yang[2]

Received: 5 September 2021 / Accepted: 13 June 2022 / Published online: 11 July 2022

Abstract

Low earth orbit satellites (LEOs) play an important role in communications, Earth observation and other applications. The real-time precise orbit determination (RTPOD) of LEOs plays an important role. However, the quality of carrier observations must be strictly controlled for the RTPOD of LEO satellites. Nevertheless, the ionospheric residual (IR) calculated from dual-frequency carrier observations at low sampling rates varies greatly due to the high speed of LEO satellites, and adopting the existing quality control method constrains the RTPOD performance in the highly dynamic environment. We present a new quality control for the receiver clock offset (QCCLK) algorithm, which combines LEO satellites' dynamic models with GNSS observations to detect carrier observation anomalies. Based on the QCCLK algorithm, real-time multi-GNSS automatic precise orbit determination (RTMG-APOD) software is designed. For comparison, we study the IR distribution at different sampling rates, revealing that the IR algorithm is not suitable for the quality control of LEO observations. RTMG-APOD software is used to analyze the RTPOD performance of the GFZ multi-GNSS final product (GBM), CNES real-time product (CNT) and IGS real-time service (RTS) product on GRACE Follow-On Level-1A observations. The RTPOD experiment results demonstrate that the 3D RMS of the GBM product is approximately 8 cm, and that of the CNT and RTS products is approximately 10 cm. Finally, an RTPOD experiment with one month of observations at different sampling rates using the GBM product and CNT real-time ephemeris verifies the stability of the QCCLK algorithm and its applicability to devices with low sampling rates.

Keywords Real-time precise orbit determination (RTPOD) · QCCLK · LEO satellites · GRACE Follow-on (GRACE-FO) · State-space representation (SSR)

Introduction

With orbit altitudes ranging approximately from 300 to 1500 km, low earth orbit (LEO) satellites can collect information on land, the atmosphere, gravity and the oceans across a large scale and perform some special services, including relay communication and space experiments (Montenbruck and Gill 2000). The gravity recovery and climate experiment follow-on (GRACE-FO) mission comprises a pair of gravity satellites, namely GRACE-FO-C and GRACE-FO-D, jointly launched in May 2018 by the National Aeronautics and Space Administration (NASA) and GeoForschungZentrum (GFZ). Equipped with high-quality GPS receivers, a K-band ranging (KBR) system and a laser ranging interferometer (LRI), GRACE-FO was designed to detect the time-varying gravitational field and average gravitational field of Earth (Kang et al. 2020). Scholars have performed considerable research on the precise orbit determination (POD) of LEO satellites by

✉ Genyou Liu
liugy@whigg.ac.cn

✉ Jikun Ou
ojk@whigg.ac.cn

[1] School of Communications and Information Engineering and School of Artificial Intelligence, Xi'an University of Posts and Telecommunications, Xi'an 710121, China

[2] State Key Laboratory of Geodesy and Earth's Dynamics, Innovation Academy for Precision Measurement Science and Technology, Chinese Academy of Sciences, Wuhan 430077, China

[3] School of Computer and Information Engineering, Xiamen University of Technology, Xiamen 361024, China

using the final ephemeris product. The use of dual-frequency global navigation satellite system (GNSS) observations and international GNSS service (IGS) final products can achieve a centimeter-level post-processing POD accuracy (Feng 2001; Kang et al. 2006). The real-time precise orbit determination (RTPOD) can be performed with relatively small latency (in a few seconds) using communication satellites (Iridium satellite or Globalstar constellation) or tracking and data relay satellite system (TDRSS) to transmit LEO observations to the ground or IGS RTS to LEO satellites. According to the tasks of LEO satellites, two orbit determination schemes can be adopted: (1) real-time autonomous orbit determination on the spaceborne platform and (2) RTPOD in the ground system after obtaining the LEO observations. Herein, we focus mainly on the second scheme.

The development of remote sensing technology and spaceborne real-time autonomous orbit determination has raised the demand for the real-time orbit determination (RTOD) of LEO satellites. In the future, RTPOD could serve to augment LEO navigation. Currently, spaceborne dual-frequency receivers use the IGS final ephemeris to perform LEO satellite POD with centimeter-scale accuracy, whereas the accuracy of spaceborne RTOD with broadcast ephemeris reaches approximately the decimeter scale (Bertiger et al. 2010; Mao et al. 2019). MetOp, a meteorological satellite managed by the European Space Agency (ESA) and the European Organisation for the Exploitation of Meteorological Satellites (EUMETSAT), can use high-quality dual-frequency GPS receivers to achieve a post-processing accuracy of 5 cm (Marquardt et al. 2007; Montenbruck et al. 2008). In addition, the Goddard Space Flight Center (GSFC) has conducted research on RTOD algorithms and developed software for spaceborne RTOD called the GPS enhanced orbit determination experiment (GEODE). Furthermore, NASA's Jet Propulsion Laboratory (JPL) developed the RTOD software GIPSY (RTG) (Reichert et al. 2002). These software programs can determine the real-time orbits of LEO satellites with an accuracy of approximately 1 m.

Montenbruck and Ramos-Bosch (2008) used the IGS ultra-rapid product and JPL real-time ephemeris to determine the orbits of different LEO satellites with accuracies of approximately 0.40 m and 0.12 m. At present, the IGS and various analysis centers (ACs) provide different precise orbit and clock offset products, including the final product, rapid product and ultra-rapid product. The IGS final product and rapid product of the orbit and clock offset have delays of approximately 12–18 days and 17–41 h, respectively, to obtain data. Moreover, the root mean square (RMS) orbit accuracy is approximately 2.50 cm, and the RMS satellite clock offset accuracy is approximately 75 ps. In contrast, the IGS ultra-rapid product has no latency in the RTOD of LEO satellites and achieves an RMS orbit accuracy of approximately 5 cm and an RMS satellite clock offset accuracy of approximately 3 ns (IGS International GNSS Service 2020; Ye et al. 2019). To meet the requirements of real-time high-precision positioning and some applications, the IGS established the real-time working group (RTWG) to develop a real-time data stream in 2001 and started to offer the IGS real-time service (RTS) in April 2013 (Hadas and Bosy 2015; Zhang et al. 2018). The RTS offered by the IGS real-time pilot project (RTPP) includes a product of the real-time dual-frequency GNSS orbit and the satellite clock offset correction; these real-time products are encoded into the radio technical commission for maritime services (RTCM) format and use networked transport of RTCM via internet protocol (NTRIP) for network transmission. Fortunately, RTS can be used for both the precise point positioning (PPP) and the RTPOD of LEO satellites (Kazmierski et al. 2018). However, to achieve stable RTPOD for LEO satellites, the quality control of spaceborne GNSS observations is particularly important.

This study is devoted to researching the RTPOD algorithm and real-time quality control of spaceborne carrier observations. Because spaceborne receivers are affected by the high-speed operating environment (that is, direct observations of the ionosphere can vary considerably between adjacent observation times), the quality control of the ionospheric residual (IR) is no longer suitable in this environment. Therefore, we propose a new method, the quality control for the receiver clock offset (QCCLK) algorithm, which can perform well in the highly dynamic environment of RTPOD. To process GNSS observations, several common quality control methods are used, including detecting the gross error by filtering residuals and detecting cycle slips by the Hatch–Melbourne–Wübbena (HMW) combination and IRs (Hatch 1982; Blewitt 1990). The IR method, which is based on the hypothesis that changes in the ionosphere between adjacent observation times are relatively small, is an effective technique in the ground-based GNSS observation environment and can detect 1 or even 0.5 cycle slips. Thus, based on adopting the new QCCLK algorithm for LEO satellite observations, we designed a new RTPOD scheme that employs the real-time data stream product (CLK93) released by the Centre National d'Études Spatiales (CNES) to perform the RTPOD of GRACE-FO spaceborne receivers. To meet the needs of spaceborne receivers in the RTPOD of multi-GNSS and multi-frequency observations, based on the cross-platform Qt (www.qt.io) framework, real-time multi-GNSS automatic precise orbit determination (RTMG-APOD) software is developed in the C++ programming language.

Real-time precise orbit and clock recovery

RTS products are usually encoded into a state-space representation (SSR) correction stream in RTCM format and broadcast to users around the world by applying NTRIP. RTS products can be obtained through IGS ACs, such as the IGS Central Bureau (IGSCB), Bundesamt für Kartographie und Geodäsie (BKG) and CNES. The real-time SSR can be divided into the center of mass (COM) and antenna phase center (APC) according to the reference position of the navigation satellite's orbit. The SSRs released by the IGS and other ACs are corrections to the broadcast ephemeris. First, the broadcast ephemeris is used to calculate the satellite's orbit and clock offset. Then, the SSR is utilized to correct the orbit and clock offset of the broadcast ephemeris, yielding the precise orbit and clock offset (Elsobeiey and Al-Harbi 2016; Wang et al. 2018). The reference coordinate system of the broadcast ephemeris is the earth-centered earth-fixed (ECEF) system, and the corrected reference coordinate system is the orbital coordinate system composed of radial, along-track, and cross-track components. The corrections $\partial\vec{O}(t)$ in the orbital coordinate system at the current observation time can be expressed as:

$$\partial\vec{\boldsymbol{O}}(t) = \begin{bmatrix} \partial O_r \\ \partial O_a \\ \partial O_c \end{bmatrix} + \begin{bmatrix} \dot{\delta}_r \\ \dot{\delta}_a \\ \dot{\delta}_c \end{bmatrix} \left(t - t_0\right) \tag{1}$$

where ∂O_r, ∂O_a, and ∂O_c are the radial, along-track and cross-track corrections, respectively, corresponding to the reference time of the orbital coordinate system t_0 (issue of data, IOD) and $\dot{\delta}_r$, $\dot{\delta}_a$ and $\dot{\delta}_c$ are the radial, along-track and cross-track change rates (these parameters can be obtained from a real-time data stream), respectively. Then, we calculate $\vec{\boldsymbol{e}}_r$, $\vec{\boldsymbol{e}}_a$, $\vec{\boldsymbol{e}}_c$, namely the radial, along-track and cross-track rotation vectors, respectively, to transform the orbital coordinate system to the ECEF coordinate system:

$$\partial\vec{\boldsymbol{X}}(t) = \left[\vec{\boldsymbol{e}}_r\vec{\boldsymbol{e}}_a\vec{\boldsymbol{e}}_c\right]\partial\vec{\boldsymbol{O}}(t) \tag{2}$$

$$\vec{\boldsymbol{e}}_a = \frac{\dot{\boldsymbol{r}}}{|\dot{\boldsymbol{r}}|}\vec{\boldsymbol{e}}_c = \frac{\boldsymbol{r}\times\dot{\boldsymbol{r}}}{|\boldsymbol{r}\times\dot{\boldsymbol{r}}|}\vec{\boldsymbol{e}}_r = \vec{\boldsymbol{e}}_a \times \vec{\boldsymbol{e}}_c \tag{3}$$

where $\partial\vec{\boldsymbol{X}}(t)$ indicates the correction for calculating the orbit of the broadcast ephemeris under the ECEF coordinate system, $\partial\vec{\boldsymbol{O}}(t)$ indicates the correction corresponding to t in the orbital coordinate system, and $\boldsymbol{r}$ and $\dot{\boldsymbol{r}}$ indicate the position and velocity of the satellite, respectively, calculated by the broadcast ephemeris under the ECEF coordinate system. Using the orbit correction $\partial\vec{\boldsymbol{X}}(t)$ to correct the orbit of the broadcast ephemeris $\overrightarrow{\boldsymbol{X}_{\boldsymbol{b}}}(t)$, the precise orbit $\overrightarrow{\boldsymbol{X}_{\boldsymbol{p}}}(t) = \overrightarrow{\boldsymbol{X}_{\boldsymbol{b}}}(t) - \partial\vec{\boldsymbol{X}}(t)$ can be obtained.

The ∂C (unit: m) corrections relative to the broadcast ephemeris dt_b (unit: s) of the observation time t can be calculated by the following formula:

$$\partial C = C_0 + C_1\left(t - t_0\right) + C_2\left(t - t_0\right)^2 \tag{4}$$

where C_0, C_1, and C_2 indicate the correction coefficient corresponding to the reference time t_0 (IOD) of the satellite clock offset. The satellite's precise clock offset dt_p corresponding to the observation time t can be calculated as follows:

$$dt_p = dt_b + \frac{\partial C}{c} \tag{5}$$

where dt_p indicates the precise satellite clock offset at the time of observation, dt_b indicates the calculated clock offset of the broadcast ephemeris, and c indicates the speed of light.

Dynamic model of LEO satellites

The forces applied to LEO satellites can be divided into conservative forces and nonconservative forces. Conservative forces include the Earth's gravity, nonspherical gravity, N-body gravity (such as gravity imposed by the Sun and Moon), solid tides, ocean tides, and polar tides, whereas nonconservative forces include atmospheric drag, solar radiation pressure, and Earth radiation pressure. Conservative forces are related only to the satellite position and can be accurately calculated by a dynamic model. In contrast, nonconservative forces are difficult to model accurately, as they are related to not only the satellite position and velocity but also many other parameters. When combining dynamic models and GNSS observations, it is necessary to frequently set some empirical model parameters to absorb the empirical forces that cannot be modeled. The motion equation of a LEO satellite in the inertial coordinate system can be expressed in the following form (Jäggi et al. 2006; Wang et al. 2015):

$$\ddot{\boldsymbol{r}} = -GM\frac{\boldsymbol{r}}{r^3} + \boldsymbol{a}_{\boldsymbol{c}}(t,\boldsymbol{r}) + \boldsymbol{a}_{\boldsymbol{nc}}(t,\boldsymbol{r},\dot{\boldsymbol{r}},\boldsymbol{p}) + \boldsymbol{T}\cdot\boldsymbol{a}_{\boldsymbol{e}} \tag{6}$$

where $\ddot{\boldsymbol{r}}$ indicates the total acceleration of the LEO satellite's center of mass; GM is the Earth's gravitational constant; $\boldsymbol{r}$ and $\dot{\boldsymbol{r}}$ indicate the position and velocity vectors, respectively, of the LEO satellite in the inertial system; $\boldsymbol{a}_{\boldsymbol{c}}(t,\boldsymbol{r})$ indicates the acceleration caused by conservative forces, such as the gravitational forces exerted by the Earth, Sun and Moon; $\boldsymbol{a}_{\boldsymbol{nc}}(t,\boldsymbol{r},\boldsymbol{v},\boldsymbol{p})$ indicates the acceleration caused by nonconservative forces, such as atmospheric drag and solar radiation pressure; and $\boldsymbol{p}$ indicates the coefficients related to

nonconservative forces, such as the atmospheric drag coefficient C_d and the solar radiation pressure coefficient C_r. In addition, $\boldsymbol{a_e} = \left[a_r, a_a, a_c\right]$ indicates the empirical acceleration in the radial, along-track, and cross-track directions, and $\boldsymbol{T}$ is the conversion matrix from the radial, along-track, and cross-track directions of the ECEF to the inertial system. The force parameters to be estimated in the GNSS observation equation include $\boldsymbol{a_e}$, C_d and C_r.

The RTPOD of LEO satellites requires a filtering algorithm combined a dynamic model to process the GNSS observations. The GNSS observation equation and dynamic model need to estimate the parameters as follows:

$$\boldsymbol{x} = \left(\boldsymbol{r}^T, \dot{\boldsymbol{r}}^T, C_r, C_d, \boldsymbol{a_e}^T, c\partial t, c\partial t_{ISB}, \boldsymbol{N}^T\right)^T \tag{7}$$

where ∂t indicates the LEO receiver clock offset that absorbs the hardware delay; ∂t_{ISB} indicates the inter-system bias, which represents the deviation from the clock offset of the reference receiver; and $\boldsymbol{N} = \left[N_1, \ldots, N_n\right]$ indicates the ambiguity parameter that absorbs the hardware delay.

For the filter time update, the transition matrix of the dynamic model needs to be calculated. If the parameter $\boldsymbol{y}\left(t_{i-1}\right) = \left(\boldsymbol{r}^T, \dot{\boldsymbol{r}}^T, C_r, C_d, \boldsymbol{a_e}^T\right)_{i-1}^T$ at t_{i-1} is known, then $\boldsymbol{y}\left(t_i\right) = \boldsymbol{\Phi}\left(t_i, t_{i-1}\right) \cdot \boldsymbol{y}\left(t_{i-1}\right)$ needs to be solved by numerical integration to find $\boldsymbol{\Phi}\left(t_i, t_{i-1}\right)$, and the differential equation for solving $\boldsymbol{\Phi}$ can be expressed in the following form:

$$\begin{cases} \frac{\mathrm{d}}{\mathrm{d}t}\Phi\left(t_i, t_{i-1}\right) = \frac{\partial f\left(t_i, \boldsymbol{y}\left(t_i\right)\right)}{\partial \boldsymbol{y}\left(t_i\right)} \cdot \Phi\left(t_i, t_{i-1}\right) \\ f\left(t_i, \boldsymbol{y}\left(t_i\right)\right) = \frac{\mathrm{d}}{\mathrm{d}t}\boldsymbol{y}\left(t_i\right) \\ \Phi\left(t_{i-1}, t_{i-1}\right) = \boldsymbol{I}_{n\times n} \end{cases} \tag{8}$$

where $\boldsymbol{\Phi}$ is the transition matrix of the dynamic model parameter $\boldsymbol{y}$ from t_{i-1} to t_i, $\boldsymbol{f}$ is the derivative of $\boldsymbol{y}$, and $\boldsymbol{I}$ is the identity matrix.

The RTPOD of LEO satellites uses the extended Kalman filter time update and mainly includes two parts. The estimated $\boldsymbol{x}_{i-1}^+$ at time t_{i-1} needs to be predicted to the state of $\boldsymbol{x}_i^-$ at time t_i through the transition matrix, and the covariance matrix $\boldsymbol{P}_{i-1}^+$ at time t_{i-1} is predicted to $\boldsymbol{P}_i^-$ at time t_i. $\boldsymbol{Q}_w$ indicates the transfer of noise between adjacent epochs:

$$\begin{cases} \boldsymbol{x}_i^- = \Phi\left(t_i, t_{i-1}\right) \cdot \boldsymbol{x}_{i-1}^+ \\ \boldsymbol{P}_i^- = \Phi\left(t_i, t_{i-1}\right) \cdot \boldsymbol{P}_{i-1}^+ \cdot \boldsymbol{\Phi}^{\boldsymbol{T}}\left(t_i, t_{i-1}\right) + \boldsymbol{Q}_w \end{cases} \tag{9}$$

The Kalman filtering measurement update is as follows:

$$\begin{cases} \boldsymbol{K}_i = \boldsymbol{P}_i^- \boldsymbol{H}_i^T \left(\boldsymbol{H}_i \boldsymbol{P}_i^- \boldsymbol{H}_i^T + \boldsymbol{R}\right)^{-1} \\ \boldsymbol{x}_i^+ = \boldsymbol{x}_i^- + \boldsymbol{K}_i\left(\boldsymbol{Z}_i - \boldsymbol{H}_i \boldsymbol{x}_i^-\right) \\ \boldsymbol{P}_i^+ = \left(I - \boldsymbol{K}_i \boldsymbol{H}_i\right)\boldsymbol{P}_i^- \end{cases} \tag{10}$$

where $\boldsymbol{H}_i$ indicates the GNSS observation equation, $\boldsymbol{Z}_i$ indicates the GNSS observations, $\boldsymbol{K}_i$ indicates the gain matrix, $\boldsymbol{x}_i^+$ indicates the parameter to be solved, and $\boldsymbol{P}_i^+$ indicates the updated measurement covariance.

RTPOD quality control algorithm

In the highly dynamic or ionospheric anomaly environment, the distribution of IRs at different sampling rates varies substantially; hence, the IR method cannot effectively detect cycle slips or perform the quality control of carrier observations. In other words, since the filtered carrier residual is contaminated, it is impossible to effectively control the quality of the carrier observations. Therefore, we present a new quality control method, the QCCLK algorithm, which combines dynamic models and GNSS observations based on the stable physical characteristics of ambiguity and the similarity of the receiver clock offset among each navigation satellite to detect the quality of the carrier observations. The QCCLK algorithm is designed to perform well in LEO RTPOD and is more suitable for spaceborne equipment with low sampling rates, such as 30 s (0.033 Hz) and 60 s (0.017 Hz). In contrast, the IR method cannot adequately detect the cycle slips of LEO satellites; moreover, although the HMW combination is not affected by the ionosphere, it can be used to detect only large cycle slips.

Montenbruck and Ramos-Bosch (2008) used predicted LEO satellites' positions and carrier ambiguities to estimate new carrier observations under the assumption that the receiver clock offset remains unchanged over a short interval. Here, we no longer assume that the receiver clock offset remains unchanged between adjacent observation times and instead use $\Delta \boldsymbol{t}_{r,i}^s$, the receiver clock offset difference calculated between the navigation satellite carrier observations of adjacent epochs, as an indicator for the quality control of GNSS observations. The QCCLK algorithm uses a dynamic model to perform a short-term forecast of the LEO position ($\boldsymbol{r}_{r,i}$) and utilizes GNSS observations to calculate the corresponding receiver clock difference ($d\boldsymbol{t}_{r,i}^s$) of each navigation satellite. Algorithm 1 in the Appendix shows the detailed calculation process of the QCCLK algorithm based on the characteristics of the receiver clock offset. The satellite receiver clock offset $\Delta \boldsymbol{t}_{r,i}^s$ is calculated for each pair of adjacent epochs, and the median $\Delta t_{r,med}$ of $\Delta \boldsymbol{t}_{r,i}^s$ is found. The difference $\Delta\Delta \boldsymbol{t}_{r,i}^s$ between $\Delta \boldsymbol{t}_{r,i}^s$ and $\Delta t_{r,med}$ is calculated, and whether $\Delta \boldsymbol{t}_{r,i}^s$ is abnormal is determined according to a given threshold σ_t (usually set to 6–8 cm). Here, σ_t is the maximum difference in the receiver clock offset variation that can be tolerated and is assigned according to the carrier wavelength. In the case of high-precision orbit determination, to be able to detect 0.5 cycle slips, this parameter is usually set to half the carrier wavelength. If $\Delta\Delta \boldsymbol{t}_{r,i}^s$ deviates

greatly, a cycle slip or gross error in this satellite carrier observation is considered to be present. Some key parameters can be described as follows:

$$\begin{cases} d\boldsymbol{t}^s_{r,i} = \left|\left|\boldsymbol{r}_{r,i} - \boldsymbol{r}^s_i\right|\right|_2 - \boldsymbol{L}^s_i + \boldsymbol{d}^s_i + \lambda_{IF}\boldsymbol{N}^s_{i-1} \\ \Delta\boldsymbol{t}^s_{r,i} = abs\left(d\boldsymbol{t}^s_{r,i} - d\boldsymbol{t}^s_{r,i-1}\right) \\ t_{r,med} = median\left(\Delta\boldsymbol{t}^s_{r,i}\right) \\ \Delta\Delta\boldsymbol{t}^s_{r,i} = abs\left(\Delta\boldsymbol{t}^s_{r,i} - \Delta t^s_{r,med} \cdot \boldsymbol{E}\right) \end{cases} \tag{11}$$

where s represents the navigation satellite system, i is the number of epochs, $\boldsymbol{r}_{r,i}$ is the dynamic model-predicted position of the LEO satellite, $\boldsymbol{r}^s_i$ is the GNSS satellite position, $\boldsymbol{L}^s_i$ is the ionosphere-free carrier observation, $\boldsymbol{d}^s_i$ is the GNSS error correction, $\boldsymbol{N}^s_i$ is the floating-point ambiguity, λ_{IF} is ionosphere-free carrier wavelength, $d\boldsymbol{t}^s_{r,i}$ is the receiver clock offset vector, $\Delta t_{r,med}$ is the median of $\Delta\boldsymbol{t}^s_{r,i}$, $\Delta\Delta\boldsymbol{t}^s_{r,i}$ is the change in $\Delta\boldsymbol{t}^s_{r,i}$, and $\boldsymbol{E}$ is the identity matrix. In addition, $abs(\cdot)$ denotes the absolute value of each element of the vector, and $median(\cdot)$ denotes the median of the vector.

RTMG-APOD

To meet the demands of LEO satellite research and RTOD in a multi-GNSS environment, we present the spaceborne GNSS data processing software RTMG-APOD, which is based on the secondary development of open-source software for multi-GNSS automatic precise positioning (MG-APP). We have uploaded all the MG-APP source code to the National Oceanic and Atmospheric Administration's National Geodetic Survey (NGS) site (www.ngs.noaa.gov/gps-toolbox/) and GitHub (www.github.com/xiaogongwei/mg_app) to be freely accessible to the public (Xiao et al. 2020). RTMG-APOD performs real-time data processing using the observations of two adjacent epochs for data quality detection and filtering. Spaceborne receivers use the earth rotation parameter (EOP) released in Bulletin A by the international earth rotation and reference systems service (IERS) to achieve RTPOD (Luzum et al. 2001; Ye et al. 2020). Table 1 shows the strategy for RTMG-APOD to process spaceborne GNSS data, and Fig. 1 shows the flowchart of RTMG-APOD for processing GNSS data. The generated keyhole markup language (KML) file can display the LEO satellite tracks on Google Earth.

Table 1 RTMG-APOD strategy for the GNSS data processing of LEO RTPOD (the predicted EOP can be downloaded from https://datacenter.iers.org/data/latestVersion/6_BULLETIN_A_V2013_016.txt; the SSR data saved by BKG ntrip client (BNC) software can be downloaded from https://igs.bkg.bund.de/ntrip/bnc; ISBs: inter-system biases)

Items	Processing strategies
GNSS measurement model	
Navigation constellation	GPS(default)/GLONASS/BDS/Galileo
Observation model	Ionospheric-free combination/Uncombined
Satellite orbit and clock	GBM/IGS product (automatic download) or BNC format
Cutoff mask angle	2° (default)
Observation weight	$P = \sin^2 e/\sigma^2$(σ^2 indicates the variance of pseudorange or carrier observations)
Receiver clock offset and ISBs	White noise estimation
Filtering method	Kalman (default)/square root information filter (SRIF)
Satellite and receiver antenna corrections	igs14.atx, PCO: linear interpolation, PCV bilinear interpolation
Phase wind-up model	Wu et al. (1993)
Ambiguity parameter	Floating-point ambiguity or PPPAR (under testing)
Dynamic model	
Earth gravity field	EGM2008 (Pavlis et al. 2012), using 80 × 80 for GRACE-FO
Planetary ephemeris	JPL DE405 (Standish 1998)
Atmospheric drag	Harris–Priester density model, fixed area, estimates C_d
Solar radiation pressure	Canon-ball model, fixed area, estimates C_r, conical Earth shadow
Tidal model	Solid Earth tide, ocean tide, pole tide (IERS conventions 2010, Petit and Luzum 2010)
Coordinate system	WGS84 (ECEF)/J2000 (ECI)
Precession and nutation	IAU2000A model (Capitaine et al. 2002; Mathews et al. 2002)
Earth rotation parameter	Predicted EOP in IERS Bulletin A
Empirical accelerations	Random walk estimation in radial, along-track, and cross-track

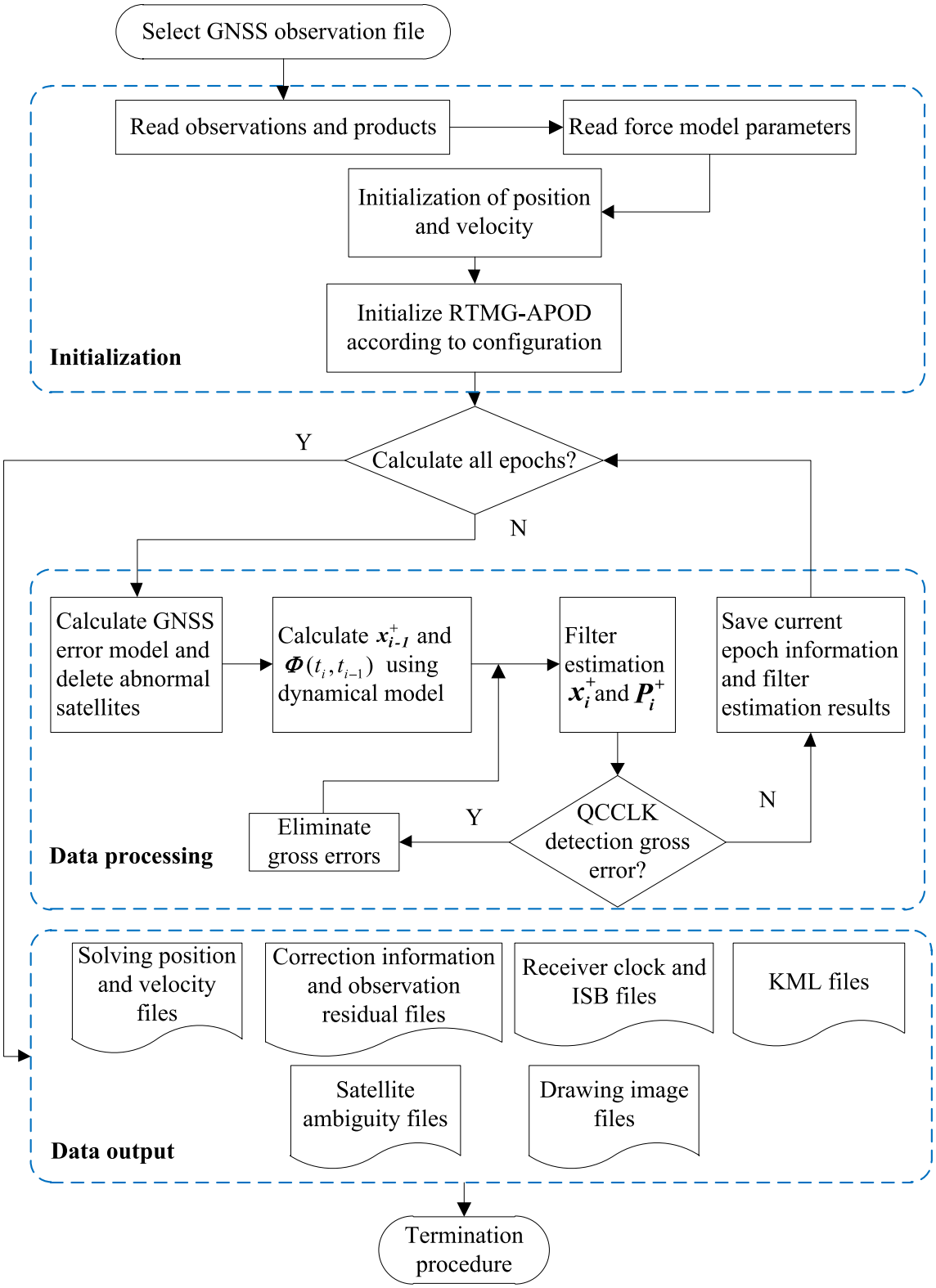

Fig. 1 Flowchart of processing GNSS measurements in the RTPOD of LEO satellites by using RTMG-APOD. The software includes three main modules: the data preparation module, data processing module, and results output module (ISB: inter-system bias; KML: keyhole markup language, which can be displayed on Google Earth)

Flight data processing and analysis

To verify the effectiveness of the QCCLK algorithm based on the characteristics of the receiver clock offset, the GPS dual-frequency observations of GRACE-FO-C Level-1A are used for an RTPOD experimental analysis. Ionosphere-free combinations can eliminate the first-order ionospheric delay, and the effects of higher-order ionospheric delays on the positioning accuracy are present only at the millimeter scale and can be ignored in centimeter-level positioning (Hoque and Jakowski 2007; Hadas et al. 2017). We download GRACE-FO-C observations from the day of year (DOY) 260 to DOY 263 in 2020 and sample them at 10 s, 30 s and 60 s for IR analysis. To conduct the RTPOD analysis (Wen et al. 2019), we employ the GRACE-FO spaceborne GPS dual-frequency observations provided by GFZ (ftp://isdcftp.gfz-potsdam.de/grace-fo/). Furthermore, we use BNC (Version 2.12.7) software to save the real-time data stream released by CNES in combination with the broadcast ephemeris provided by the crustal dynamics data information system (CDDIS, https://cddis.nasa.gov/archive/) to obtain the real-time precise orbit and clock offset. The GRACE-FO-C RTPOD experiments are conducted using the GBM products provided by GFZ (ftp://ftp.gfz-potsdam.de/) and the CNT products provided by CNES (ftp://ppp-wizard.net/) (Noll 2010; Männel et al. 2020).

Based on the developed RTMG-APOD software for the RTPOD analysis of GRACE-FO observations, the dynamic models include the following: the 2008 Earth gravitational model (EGM2008) (80 × 80) gravity field, the planetary gravitational forces of the Sun and Moon, the Harris–Priester atmospheric density model, the "canon-ball" solar radiation pressure model, the Earth tide and pole tide, and estimates of the empirical accelerations in the radial, along-cross, and cross-track directions (Hatten and Russell 2017).

Ionospheric residual distributions at different sampling rates

Geometry-free (GF) combinations eliminate all geometry-related errors and the first-order ionospheric delay, so they are ideal for detecting quality problems and inconsistencies in carrier observations. Equation (12) shows the principle of GF combinations, and equation (13) shows how the IR is calculated (Hatch 2006; Wang and Rothacher 2013):

$$\lambda_1\varphi_1(t_i) - \lambda_2\varphi_2(t_i) = \lambda_1 N_1 - \lambda_2 N_2 - \delta_{ion}(t_i) + \varepsilon_i \tag{12}$$

$$\begin{cases} IR = \delta_{ion}(t_i) - \delta_{ion}(t_{i-1}) = -(\lambda_1\Delta\varphi_1 - \lambda_2\Delta\varphi_2) + \Delta\varepsilon \\ \Delta\varphi_1 = \varphi_1(t_i) - \varphi_1(t_{i-1}) \\ \Delta\varphi_2 = \varphi_2(t_i) - \varphi_2(t_{i-1}) \\ \Delta\varepsilon = \varepsilon_i - \varepsilon_{i-1} \end{cases} \tag{13}$$

where φ_1 and φ_2 are the carrier observations, λ_1 and λ_2 are the corresponding wavelengths, t_i and t_{i-1} are the observation times, N_1 and N_2 are the ambiguity parameters, ε_i is the residual, and δ_{ion} is the ionospheric delay.

In this section, we analyze the IR distributions at sampling rates of 10 s, 30 s, and 60 s on DOYs 262 and 263 in 2020 by using GRACE-FO-C Level-1A dual-frequency GPS observations. We find that the changes in the IR at the 10 s sampling rate are within 0.1 m, while they can reach approximately 0.2 m at the 30 s sampling rate and can exceed 0.2 m at the 60 s sampling rate. In the processing of LEO satellite data, IRs are difficult to use to effectively control the quality of carrier observations. The IR distributions are shown in Fig. 2.

Figure 2 shows that because GRACE-FO-C moves periodically around the Earth, the distributions of IRs also exhibit periodicity. Moreover, the changes in the IR at different sampling rates are quite different. The residuals of the 60 s

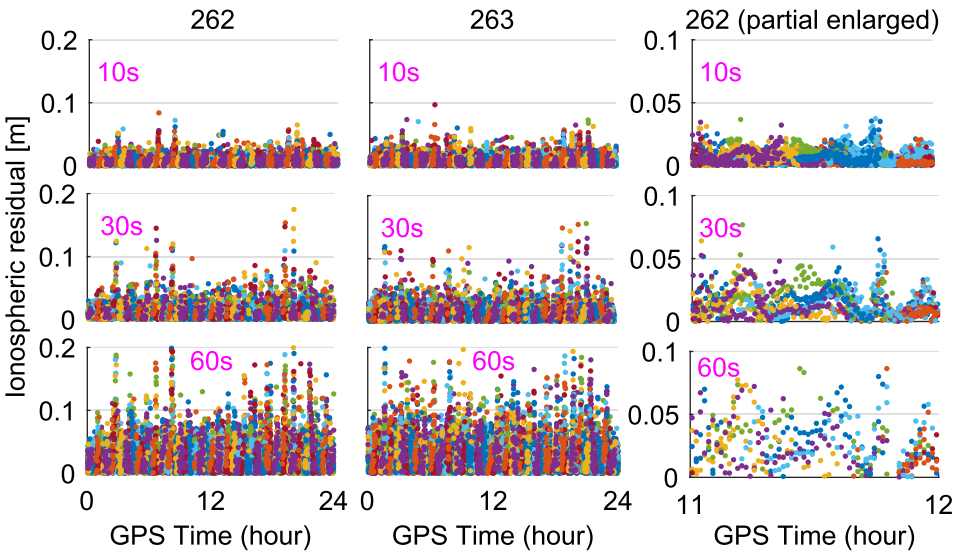

Fig. 2 GPS satellite IR distributions (the left side is for DOY 262, the middle is for DOY 263, and the right side is an enlarged view of DOY 262; the data sampling rates from top to bottom are 10 s, 30 s, and 60 s; different colors represent different GPS satellites)

observations of the GRACE-FO-C satellite's position vary greatly (the maximum value can reach 0.20 m or more), while relatively small changes are found in the 30 s observations of the GRACE-FO-C satellite's position and IR error (the maximum is approximately 0.10 m). In addition, the change in the IR of the 10 s observations is less than 0.05 m, so a fixed IR threshold can be used for the quality control preprocessing of such observations.

RTPOD experimental analysis by using QCCLK algorithm

To verify the effectiveness of the QCCLK algorithm (Algorithm 1), the real-time data stream (CLK93) issued by CNES is used to correct the broadcast ephemeris, and GRACE-FO-C Level-1A observations with a sampling rate of 30 s are processed in this section. With the new QCCLK algorithm proposed in this article, a comparative analysis is performed among the new algorithm, the IR error method with a fixed threshold of 0.2 m (IR-0.2) and the no-QCCLK and no-IR method (no-QC-IR) for carrier phase observations. If the IR error of a satellite is greater than 0.2 m, the observation of this satellite is removed. The RTPOD experiment is carried out using observations from the GRACE-FO-C satellite on DOYs 262 and 263 in 2020. The precise orbit of GRACE-FO-C in the ECEF coordinate system released by JPL is used as the reference value, and its orbit accuracy is better than 2 cm (Kornfeld et al. 2019). The radial (R), along-track (A), and cross-track (C) error curves of RTPOD on DOYs 262 and 263 are shown in Fig. 3.

Figure 3 shows that when processing spaceborne observation data, using the QCCLK algorithm can effectively control the quality of carrier observations, with the radial, along-track, and cross-track error curves fluctuating at 20 cm. When using the IR-0.2 method, the orbit determination result appears unstable, and the RTPOD on DOY 262 cannot converge stably; furthermore, although the RTPOD result on DOY 263 is better, the accuracy is not as good as that of the QCCLK algorithm. Without quality control, the determination cannot achieve stable convergence due to carrier and inadequate data quality. The RMS statistics (filtering the results after 1 h) on the radial, along-track and cross-track components and the 3D convergence on DOYs 262 and 263 using the QCCLK, IR-0.2 and no-QC-IR methods are shown in Table 2.

The carrier residual includes both modeled and unmodeled errors. Hence, the accuracy of the carrier residual is one of the main indicators in evaluating the RTOD accuracy. Figure 4 presents diagrams of the residual distributions of the ionosphere-free combination carrier observations on DOYs

Table 2 Statistics of the GRACE-FO-C RTPOD accuracy for DOYs 262 and 263 in 2020 (RMS statistics in the radial, along-track, cross-track, and 3D directions, unit: cm)

Methods	DOY	R	A	C	3D
QCCLK	262	6.39	5.98	4.70	9.93
	263	6.40	5.00	4.31	9.19
IR-0.2	262	12.69	12.75	9.30	20.25
	263	6.85	5.96	4.53	10.14
no QCCLK and IR	262	33.04	32.60	28.13	54.27
	263	29.36	27.27	19.52	44.57

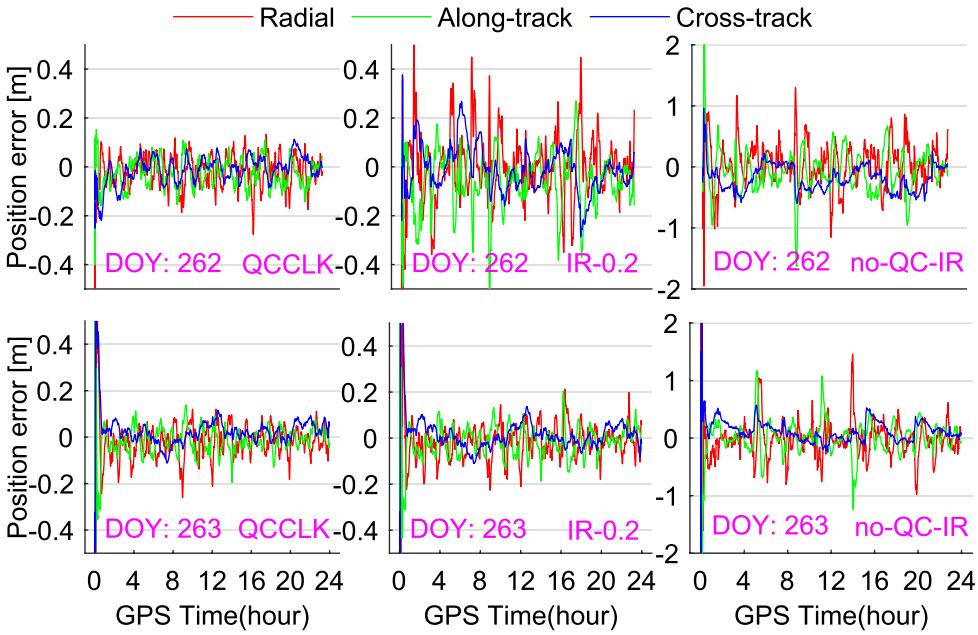

Fig. 3 Using the real-time data stream product of CNES for the RTPOD of GRACE-FO-C (from left to right are the results of the QCCLK, IR-0.2 and no-QC-IR algorithms)

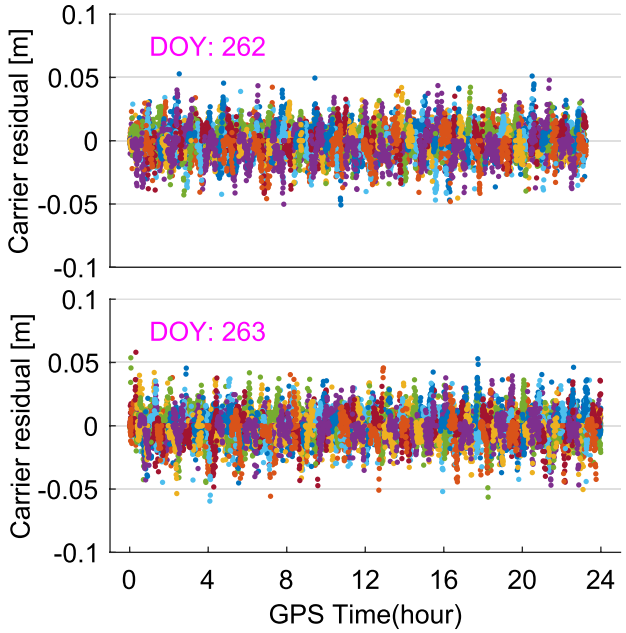

Fig. 4 Residual distributions of the ionosphere-free combination carrier observations (the top is for DOY 262, while the bottom is for DOY 263, and different colors represent different GPS satellites)

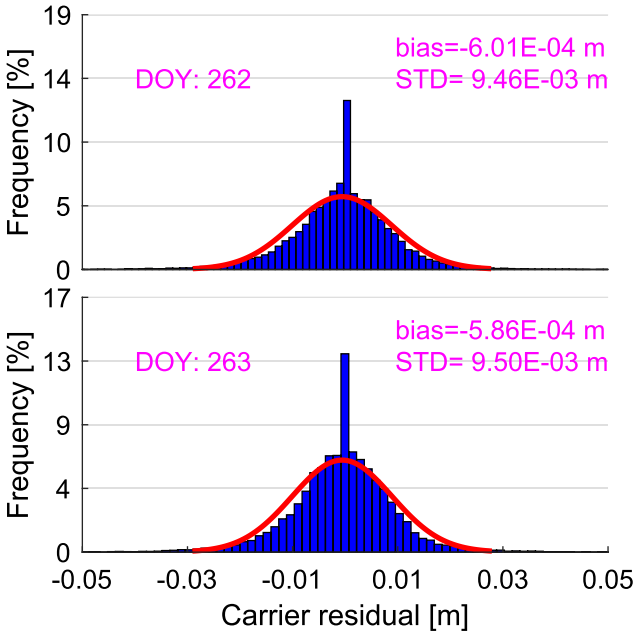

Fig. 5 Residual statistics of the ionosphere-free combination carrier observations (the top is for DOY 262, while the bottom is for DOY 263)

262 and 263 obtained with the proposed QCCLK algorithm. Figure 5 plots the distribution statistics of the carrier residuals, including the bias and standard deviation (STD).

Figure 4 shows that the distributions of the ionosphere-free combination carrier residuals are relatively concentrated within 5 cm, and Fig. 5 shows that the carrier residuals are mainly concentrated near zero, with the statistical results resembling a normal distribution. These experiments show the reliability of RTPOD with the proposed QCCLK algorithm and that this method can effectively detect carrier quality problems in the RTPOD of LEO satellites.

RTPOD using different products

The ionospheric delay can be eliminated by using dual-frequency GNSS observations. The factors that affect the accuracy of RTPOD are mainly the accuracies of the orbit and clock offset products of navigation satellites. Based on the proposed QCCLK algorithm, this section uses the GBM final product, the CNT real-time ephemeris product and the real-time data stream product (CLK93) to process the observations of the GRACE-FO-C satellite from DOY 260 to 263 (sampling rate of 30 s) for an RTPOD analysis. The GRACE-FO-C orbit calculated by RTMG-APOD is compared and analyzed with the precise orbits released by JPL, and the RTPOD error curves for different products on DOY 260 are shown in Fig. 6. To facilitate a comparative analysis of the RTPOD results, the radial, along-track, cross-track and 3D RMS statistics are computed. Table 3 shows the results of the position error and convergence time from DOY 260 to 263, and a histogram of the statistical results in Table 3 is plotted in Fig. 7. Convergence is defined by the IRs in the radial, along-track, and cross-track directions being simultaneously less than 0.2 m.

The statistics in Table 3 and Fig. 7 show that using the final GBM product to process data from GRACE-FO-C yields the highest RTPOD accuracy and the fastest convergence time. The CNT real-time ephemeris product and real-time data stream product (CLK93) achieve similar performance. Although the GRACE-FO-C satellite moves faster and the geometric structures of GPS observation satellites vary greatly, the shorter continuous observation time of GPS satellites also causes a longer convergence time.

RTPOD with different sampling rates by using the QCCLK algorithm

To verify the stability of the QCCLK algorithm and the suitability of the algorithm for equipment with a low sampling rate, we download the GRACE-FO-C Level-1A spaceborne observations from DOY 122 to 152 in 2020 for RTPOD, resample the observations to 30 s (0.033 Hz) and 60 s (0.017 Hz), and use the GBM final product and CNT real-time ephemeris to verify and analyze the RTPOD performance. One month of 30 s GRACE-FO-C observations can verify the stability of the QCCLK algorithm, and the 60 s GRACE-FO-C observations verify that the QCCLK algorithm is suitable for devices

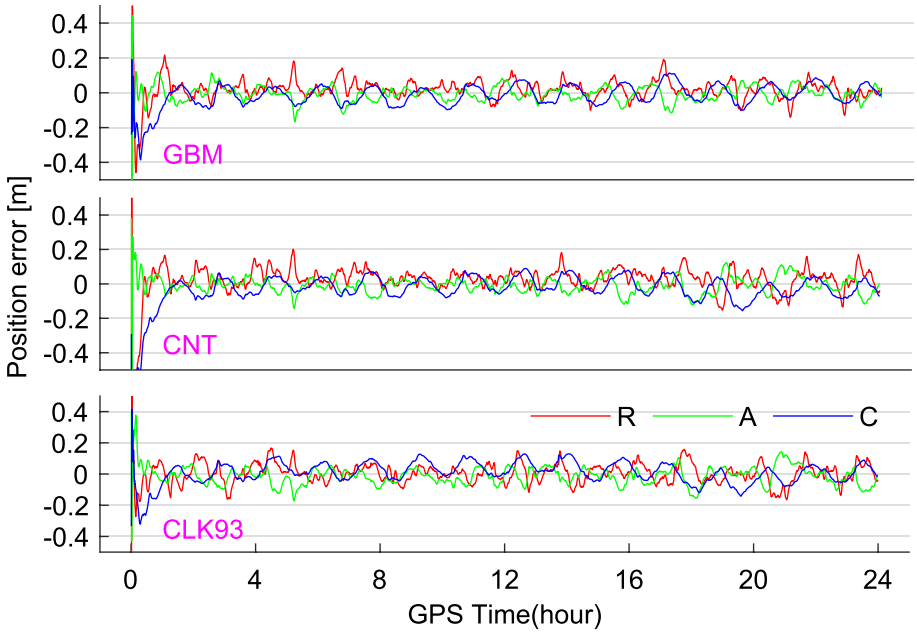

Fig. 6 Error curve of RTPOD for different products on DOY 260 (the top is the GBM final product, the middle is the CNT real-time ephemeris product, and the bottom is the real-time data stream product (CLK93))

Table 3 Statistics of the radial, along-track, and cross-track RMS (unit: cm), 3D RMS (unit: cm) and convergence time (unit: min) using different products

DOY	Products	Radial	Along-track	Cross-track	3D RMS	Convergence time
260	GBM	5.23	4.06	4.95	8.27	44.00
	CNT	6.12	4.48	5.36	9.29	48.50
	CLK93	6.03	5.48	5.91	10.06	34.50
261	GBM	4.51	4.13	5.09	7.96	17.50
	CNT	6.39	5.86	5.84	10.45	24.00
	CLK93	6.42	6.04	6.28	10.82	29.00
262	GBM	6.25	5.71	4.24	9.46	32.50
	CNT	6.74	6.01	5.34	10.49	46.50
	CLK93	6.39	5.98	4.70	9.93	48.50
263	GBM	5.40	3.85	3.82	7.66	37.00
	CNT	6.18	4.74	3.43	8.51	46.00
	CLK93	6.40	5.00	4.31	9.19	46.50

with low sampling rates. Figure 8 shows the statistics of the RTPOD 3D RMS accuracy for the GRACE-FO-C Level-1A observations by using the GBM and CNT products through histograms.

The statistical RTPOD results in Fig. 8 show a significant difference in the RTPOD accuracy between the GBM final product and CNT real-time ephemeris. The RTPOD accuracy of the GBM final product is high; the average 3D RMS is 8.58 cm (30 s) and 8.94 cm (60 s), while the average 3D RMS of the CNT real-time ephemeris is 10.54 cm (30 s) and 11.36 cm (60 s). In addition, the RTPOD accuracy of the 30 s observations is slightly higher than that of the 60 s observations. Ultimately, using one month of GRACE-FO-C spaceborne observations for RTPOD confirms the stability of the QCCLK algorithm and its suitability for RTPOD at low sampling rates. Indeed, even for spaceborne observations with a low sampling rate (60 s or 0.017 Hz), the QCCLK algorithm can still achieve RTPOD.

Conclusion

With improvements in communications technology, the use of IGS RTS products can further improve the RTPOD accuracy of LEO satellites. When transmitting spaceborne observations to the ground, the computational load of the complex dynamic model and parameter estimation can be transferred to computers on the ground, which greatly reduces the load on the

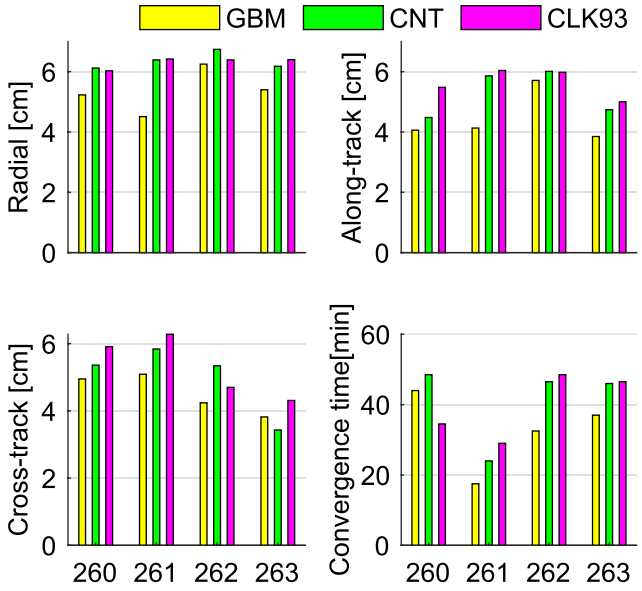

Fig. 7 RTPOD for different products in histograms of the radial, along-track, and cross-track RMS (unit: cm) and convergence time (unit: min)

spaceborne receiver. We propose a new method to detect the quality of GNSS carrier observations and conduct RTPOD on GRACE-FO-C satellites. Compared with the broadcast ephemeris, the spaceborne autonomous RTOD accuracy is approximately 0.50 m (3D RMS), and using a real-time data streaming product (CLK93) can achieve an orbit determination accuracy of 0.10 m (3D RMS).

Furthermore, the effectiveness of the QCCLK algorithm is verified by RTPOD experiments. We also use spaceborne observations to show that using a fixed IR threshold for LEO satellites cannot effectively detect the quality of carrier observations. The experiments reveal that the RTPOD accuracy (3D RMS) for GRACE-FO-C observations by using real-time data stream products is approximately 0.1 m based on the QCCLK algorithm. In contrast, if the QCCLK algorithm is not used, the RTPOD error may not converge.

Finally, the CNES real-time data stream product (CLK93), the CNT real-time ephemeris and the GBM final product are used to analyze the RTPOD performance for GRACE-FO-C. The experiment demonstrates that the average 3D RMS RTPOD accuracy of the GBM product is approximately 8 cm, while those of the CNT and CLK93 products are approximately 10 cm. Furthermore, the analysis of an RTPOD experiment using one month of data at different sampling rates shows the stability of the QCCLK algorithm and its suitability for RTPOD at low sampling rates.

Appendix

In Appendix Algorithm 1, the GNSS error corrections $\boldsymbol{d}_i$ includes navigation satellite clock offset, phase hardware delays and antenna corrections of the receiver and satellite, Earth rotation corrections, relativistic corrections, etc. The σ_r indicates the 3D LEO satellite positioning accuracy after RTPOD convergence, and the value of σ_r is generally between 5 and 10 cm when using precise orbit and clock offset product. σ_t indicates the maximum deviation of each navigation satellite from the median, which is usually 6–8 cm to detect 1 cycle or 0.5 cycle slip or gross errors. s represent the navigation satellite system,$\boldsymbol{dt}^s_{r,i}$ is receiver clock offset vector, $\Delta t_{r,med}$ is the median of $\Delta \boldsymbol{t}^s_{r,i}$.

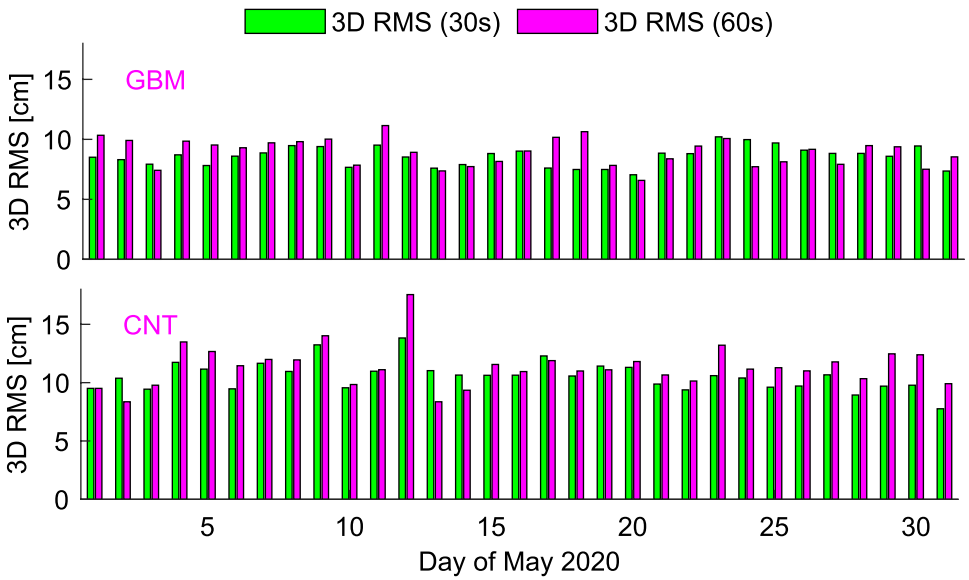

Fig. 8 Statistical histograms of the RTPOD 3D RMS (unit: cm) for 30 s and 60 s GRACE-FO-C observations using the GBM final product (top) and CNT real-time ephemeris (bottom)

Algorithm 1 Quality control algorithm using receiver clock offset for LEO RTPOD

Task: Quality control (QC) for GNSS phase observation of LEO RTPOD.

Parameters: Predicted LEO position $\boldsymbol{r}_{r,i}$, ionosphere-free carrier observation $\boldsymbol{L}_i^s$, GNSS error corrections $\boldsymbol{d}_i^s$, receiver clock offset $d\boldsymbol{t}_{r,i}^s$, ionosphere-free floating-point ambiguity $\boldsymbol{N}_i^s$, ionosphere-free carrier wavelength λ_{IF}, GNSS satellite position $\boldsymbol{r}_i^s$, epoch number i, position threshold σ_r, position covariance matrix $\boldsymbol{P}_i^+$, satellite navigation system s, receiver clock offset threshold σ_t, $\boldsymbol{P}_i^+$ dimension m.

Initialization: $i = 1$, $\boldsymbol{P}_0^+ = +\infty$, calculate $\boldsymbol{r}_{r,0}$, $d\boldsymbol{t}_{r,0}^s$ and $\boldsymbol{N}_0^s$ using SPP (single point positioning) of code and phase combination

Iteration: **for** $i = 1 \ldots$ **do**

if $\sqrt{\sum_{j=1}^{m} \boldsymbol{P}_i^+(j)^2} < \sigma_r$ **then**

$d\boldsymbol{t}_{r,i}^s = \left\| \boldsymbol{r}_{r,i} - \boldsymbol{r}_i^s \right\|_2 - \boldsymbol{L}_i^s + \boldsymbol{d}_i^s + \lambda_{IF}\boldsymbol{N}_{\boldsymbol{i-1}}^s$

$\Delta\boldsymbol{t}_{r,\boldsymbol{i}}^s = abs(d\boldsymbol{t}_{r,i}^s - d\boldsymbol{t}_{r,i-1}^s)$, $\Delta t_{r,med} = median(\Delta\boldsymbol{t}_{r,i}^s)$
($abs(\cdot)$ is the absolute value of each element of the vector, and $median\ (\cdot)$ is the median of the vector)

$\Delta\Delta\boldsymbol{t}_{r,\boldsymbol{i}}^{\boldsymbol{s}} = abs(\Delta\boldsymbol{t}_{r,\boldsymbol{i}}^s - \Delta t_{r,med}^s \cdot \boldsymbol{E})$

if $\Delta\Delta\boldsymbol{t}_{r,\boldsymbol{i}}^{\boldsymbol{s}}(k) > \sigma_t$ **then**

delete the k-th satellite (k is index of $\Delta\Delta\boldsymbol{t}_{r,\boldsymbol{i}}^{\boldsymbol{s}}$)

end if

use filtering algorithm to solve equation and update $\boldsymbol{P}_i^+$

else

continue;

end if

end for

Output: Save calculation results to files.

Acknowledgements We would like to thank the GFZ, CNES, JPL and CDDIS for providing GRACE-FO spaceborne observations and products, and BKG for its BNC software. In addition, we are grateful to Ming Gao, Shengliang Wang, Dong lv, and Xiacheng Li for their help. We also appreciate the reviewers for their valuable suggestions on improving the manuscript. This work is funded by the National Natural Science Foundation of China (Nos. 41974008, 41574015, 41774017, and 41804019) and the National Key Research Programme of China Collaborative Precision Positioning Project (No. 2016YFB0501900).

Data availability In this paper, we use the GRACE-FO Level-1A spaceborne GPS dual-frequency observations provided by GFZ, the GRACE-FO precise orbit released provided by JPL (ftp://isdcftp.gfz-potsdam.de/grace-fo/), the broadcast ephemeris provided by CDDIS (https://cddis.nasa.gov/archive/gps/data/daily/), the GBM precise orbit and clock offset product provided by GFZ (ftp://ftp.gfz-potsdam.de//pub/home/GNSS/products/mgex/), the CNT real-time ephemeris provided by CNES (ftp://ppp-wizard.net//PRODUCTS/REAL_TIME/), and real-time service (RTS) can be saved by BNC software (https://igs.bkg.bund.de/ntrip/bnc).

References

Bertiger W, Desai SD, Dorsey A, Haines BJ, Harvey N, Kuang D, Sibthorpe A, Weiss JP (2010) Sub-centimeter precision orbit determination with GPS for ocean altimetry. Mar Geod 33(S1):363–378. https://doi.org/10.1080/01490419.2010.487800

Blewitt G (1990) An automatic editing algorithm for GPS data. Geophys Res Lett 17(3):199–202. https://doi.org/10.1029/GL017i003p00199

Capitaine N, Gambis D, McCarthy D, Petit G, Ray J, Richter B, Rothacher M, Standish M, Vondrak J (eds) (2002) IERS technical note

29 proceedings of the IERS workshop on the implementation of the new IAU resolutions 2002. Verlag des Bundesamts für Kartographie und Geodasie, Frankfurt am Main

Elsobeiey M, Al-Harbi S (2016) Performance of real-time precise point positioning using IGS real-time service. GPS Solut 20(3):565–571. https://doi.org/10.1007/s10291-015-0467-z

Feng Y (2001) An alternative orbit integration algorithm for GPS-based precise LEO autonomous navigation. GPS Solut 5:1–11. https://doi.org/10.1007/PL00012882

Hadas T, Bosy J (2015) IGS RTS precise orbits and clocks verification and quality degradation over time. GPS Solut 19(1):93–105. https://doi.org/10.1007/s10291-014-0369-5

Hadas T et al (2017) Impact and implementation of higher-order ionospheric effects on precise GNSS applications. J Geophys Res Solid Earth 122(11):9420–9436. https://doi.org/10.1002/2017JB014750

Hatch R (1982) The synergism of GPS code and carrier measurements. In: Proceeding of third international symposium on satellite doppler positioning physical science laboratory, New Mexico Stat University, vol 2, pp 1213–1231

Hatch R (2006) A new three-frequency, geometry-free, technique for ambiguity resolution. In: Proceeding of ION GNSS, 26–29 September, Fort Worth, TX, pp 309–316

Hatten N, Russell RP (2017) A smooth and robust Harris–Priester atmospheric density model for low Earth orbit applications. Adv Space Res 59(2):571–586. https://doi.org/10.1016/j.asr.2016.10.015

Hoque MM, Jakowski N (2007) Higher order ionospheric effects in precise GNSS positioning. J Geod 81(4):259–268. https://doi.org/10.1007/s00190-006-0106-0

IGS International GNSS Service (2021) http://www.igs.org/products. Accessed 10 Aug 2021

Jäggi A, Hugentobler U, Beutler G (2006) Pseudo-stochastic orbit modeling techniques for low-Earth orbiters. J Geod 80(1):47–60. https://doi.org/10.1007/s00190-006-0029-9

Kang Z, Bettadpur S, Nagel P, Save H, Poole S, Pie N (2020) GRACE-FO precise orbit determination and gravity recovery. J Geod 94:1–17. https://doi.org/10.1007/s00190-020-01414-3

Kang Z, Tapley B, Bettadpur S, Ries J, Nagel P, Pastor R (2006) Precise orbit determination for the GRACE mission using only GPS data. J Geod 80(6):322–331. https://doi.org/10.1007/s00190-006-0073-5

Kazmierski K, Sośnica K, Hadas T (2018) Quality assessment of multi-GNSS orbits and clocks for real-time precise point positioning. GPS Solut 22(1):1–12. https://doi.org/10.1007/s10291-017-0678-6

Kornfeld RP, Arnold BW, Gross AMA et al (2019) GRACE-FO: The gravity recovery and climate experiment follow-on mission. J Spacecr Rocket 56:931–951. https://doi.org/10.2514/1.A34326

Luzum BJ, Ray JR, Carter MS, Josties FJ (2001) Recent improvements to IERS bulletin a combination and prediction. GPS Solut 4(3):34–40. https://doi.org/10.1007/PL00012853

Mao X, Visser P, van den IJssel J (2019) Absolute and relative orbit determination for the CHAMP/GRACE constellation. Adv Space Res 63(12):3816–3834. https://doi.org/10.1016/j.asr.2019.02.030

Männel B, Brandt A, Nischan T., Brack A, Sakic P, Bradke M (2020) GFZ final product series for the International GNSS Service (IGS). GFZ Data Services. https://doi.org/10.5880/GFZ.1.1.2020.002

Mathews PM, Herring TA, Buffet B (2002) Modeling of nutation-precession: new nutation series for nonrigid Earth, and insights into the Earth's interior. J Geophys Res. https://doi.org/10.1029/2001jb000390

Montenbruck O, Gill E (2000) Satellite orbits: models, methods and applications. Springer, Heidelberg

Montenbruck O, Ramos-Bosch P (2008) Precision real-time navigation of LEO satellites using global positioning system measurements. GPS Solut 12:187–198. https://doi.org/10.1007/s10291-007-0080-x

Montenbruck O, Andres Y, Bock H, van Helleputte T, van den Ijssel J, Loiselet M, Marquardt C, Silvestrin P, Visser P, Yoon Y (2008) Tracking and orbit determination performance of the GRAS instrument on MetOp-A. GPS Solut 12:289–299. https://doi.org/10.1007/s10291-008-0091-2

Noll CE (2010) The crustal dynamics data information system: a resource to support scientific analysis using space geodesy. Adv Space Res 45(12):1421–1440. https://doi.org/10.1016/j.asr.2010.01.018

Pavlis NK, Holmes SA, Kenyon SC, Factor JK (2012) The development and evaluation of the earth gravitational model 2008 (EGM2008). J Geophys Res Solid Earth. https://doi.org/10.1029/2011JB008916

Petit G, Luzum B (2010) IERS conventions 2010 (IERS Techni-cal Note; 36). Frankfurt am Main: Verlag des Bundesamts für Kartographie und Geodäsie, 2010, p 179. ISBN: 3-89888-989-6

Reichert A, Meehan T, Munson T (2002) Toward decimeter-level real-Time orbit determination:A demonstration using the SAC-C and CHAMP spacecraft. In: Proceedings of ION GNSS, 24–27 September, Portland City, OR

Standish E (1998) JPL planetary and lunar ephemerides DE405/LE405. Interoffice Memorandum IOM 312.F-98-048. Jet Propulsion Laboratory, Pasadena

Marquardt C, Andres Y, von Engeln A, Clerigh EO, Sancho F (2007) GRAS on Metop: data quality. In: Proceedings of second FORMOSAT-3/COSMIC data users workshop, Boulder, Colorado, 22–24 October 2007

Wu JT, Wu SC, Hajj GA, Bertiger WI, Lichten SM (1993) Effects of antenna orientation on GPS carrier phase. Manuscr Geod 18(2):91–98

Wang K, Rothacher M (2013) Ambiguity resolution for triple-frequency geometry-free and ionosphere-free combination tested with real data. J Geod 87(6):539–553. https://doi.org/10.1007/s00190-013-0630-7

Wang F, Gong X, Sang J, Zhang X (2015) A novel method for precise onboard real-time orbit determination with a standalone GPS receiver. Sensors 15(12):30403–30418. https://doi.org/10.3390/s151229805

Wang Z, Li Z, Wang L, Wang X, Yuan H (2018) Assessment of multiple GNSS real-time SSR products from different analysis centers. ISPRS Int J Geo Inf 7(3):85. https://doi.org/10.3390/ijgi7030085

Wen HY, Kruizinga G, Paik M, Landerer F, Bertiger W, Sakumura C, Bandikova T, Mccullough C (2019) Gravity recovery and climate experiment follow-on (GRACE-FO). Level-1 data product user handbook vol JPL D-56935 (URS270772)

Xiao G, Liu G, Ou J, Liu G, Wang S, Guo A (2020) MG-APP: an open-source software for multi-GNSS precise point positioning and application analysis. GPS Solut 24(66):1–13. https://doi.org/10.1007/s10291-020-00976-1

Ye F, Yuan Y, Tan B, Deng Z, Ou J (2019) The preliminary results for five-system ultra-rapid precise orbit determination of the one-step method based on the double-difference observation model. Remote Sens 11(1):46. https://doi.org/10.3390/rs11010046

Ye F, Yuan Y, Deng Z (2020) Improved ultra-rapid UT1-UTC determination and its preliminary impact on GNSS satellite ultra-rapid orbit determination. Remote Sens 12(3584):3584. https://doi.org/10.3390/rs12213584

Zhang L, Yang H, Gao Y, Yao Y, Xu C (2018) Evaluation and analysis of real-time precise orbits and clocks products from different IGS analysis centers. Adv Space Res 61(12):2942–2954. https://doi.org/10.1016/j.asr.2018.03.029

Gongwei Xiao received the M.S. degree from the College of Geodesy and Geomatics, Shandong University of Science and Technology in 2018, and received Ph.D. from State Key Laboratory of Geodesy and Earth Dynamics, Innovation Academy for Precision Measurement Science and Technology, Chinese Academy of Sciences (CAS), in 2021. He is now working as a lecturer with the Xi'an University of Posts and Telecommunications. His current research mainly focuses on multi-GNSS PPP, real-time precise orbit determination for LEO satellites and tropospheric delay. To meet the demands of research and precise point positioning (PPP) in a multi-GNSS environment, he open-sourced a GNSS data processing software named MG-APP (https://geodesy.noaa.gov/gps-toolbox/; https://github.com/xiaogongwei/MG_APP).

Genyou Liu received M.S. and Ph.D. from the Institute of Geodesy and Geophysics (IGG), Chinese Academy of Sciences (CAS), in 1992 and 2004, respectively. He is now working as a professor and doctoral supervisor in the State Key Laboratory of Geodesy and Earth Dynamics of Innovation Academy for Precision Measurement Science and Technology, Chinese Academy of Sciences. His areas of interest are GNSS positioning, orbit determination.

Jikun Ou received M.S. and Ph.D. from the Institute of Geodesy and Geophysics (IGG), Chinese Academy of Sciences (CAS), in 1982 and 1994. He is a research professor and a doctoral supervisor in the State Key Laboratory of Geodesy and Earth Dynamics of Innovation Academy for Precision Measurement Science and Technology, CAS. His researches include the control of data quality, detection of gross errors, and precise orbit determination for LEO and GNSS satellites.

Chongchong Zhou received his Ph.D. in State Key Laboratory of Geodesy and Earth Dynamics, Innovation Academy for Precision Measurement Science and Technology of CAS, Wuhan, China. He currently works as an engineer in the National Geodetic Observatory, Innovation Academy for Precision Measurement Science and Technology of CAS, Wuhan, China. His main research interests focus on precise orbit determination of LEOs, DORIS.

Zaimin He received M.S. and Ph.D. from National Time Service Center (NTSC), Chinese Academy of Sciences (CAS), in 2008 and 2012, respectively. He is now working as a professor and master supervisor in Xi'an University of Posts & Telecommunications. His main research interests are focused on radio positioning, timing, and communication.

Runjing Chen received his Ph.D. in 2014 from the Institute of Geodesy and Geophysics (IGG), Chinese Academy of Sciences (CAS), Wuhan, China. He currently works as a lecturer in the School of Computer and Information Engineering at Xiamen University of Technology. His research interests include GNSS data processing, precise orbit determination of LEO satellites and GNSS applications in space geodesy.

Aizhi Guo received a Ph.D. in Geodesy and Surveying in 2013 from the Institute of Geodesy and Geophysics (IGG), Chinese Academy of Sciences (CAS). Now he is an associate professor in the State Key Laboratory of Geodesy and Earth's Dynamics of IGG, CAS. His research interests include GNSS Seismology, GNSS precise positioning, deformation monitoring.

Zhouming Yang received the M.S. degree from the College of Geodesy and Geomatics, Shandong University of Science and Technology, Qingdao, China, in 2021 and is currently a Ph.D. student at State Key Laboratory of Geodesy and Earth Dynamics, Innovation Academy for Precision Measurement Science and Technology, Chinese Academy of Sciences (CAS), Wuhan, China. His current research mainly focuses on low earth orbiting satellite precise orbit determination and GNSS applications.